Journal of Materials Sciences and Applications
2018; 4(1): 10-16
http://www.aascit.org/journal/jmsa
ISSN: 2381-0998 (Print); ISSN: 2381-1005 (Online)

American Association for Science and Technology

Keywords
XAFS Cumulant,
Thermal Expansion Coefficient,
Correlated Einstein Model,
Hcp Crystals

Received: January 8, 2018
Accepted: January 20, 2018
Published: February 5, 2018

Advances in Theoretical and Experimental XAFS Studies of Debye-Waller Factor and Thermal Expansion Coefficient of Hcp Crystals

Tong Sy Tien[1], Nguyen Ba Duc[2], Ha Dang Khoa[3], Nguyen Van Hung[4,*]

[1]Department of Basic Sciences, University of Fire Fighting & Prevention, Hanoi, Vietnam
[2]Department of Physics, Tan Trao University, Tuyen Quang, Vietnam
[3]School of Engineering Physics, Hanoi University of Science and Technology, Hanoi, Vietnam
[4]Department of Physics, VNU Hanoi University of Science, Hanoi, Vietnam

Email address
hungnv@vnu.edu.vn (N. V. Hung)
[*]Corresponding author

Citation
Tong Sy Tien, Nguyen Ba Duc, Ha Dang Khoa, Nguyen Van Hung. Advances in Theoretical and Experimental XAFS Studies of Debye-Waller Factor and Thermal Expansion Coefficient of Hcp Crystals. *Journal of Materials Sciences and Applications.* Vol. 4, No. 1, 2018, pp. 10-16.

Abstract
Theoretical and experimental Debye-Waller factors presented in terms of cumulant expansion and thermal expansion coefficient in X-ray absorption fine structure (XAFS) of hcp crystals have been studied. The advances in these studies are shown by a derived method using that the calculations and measurements are necessary only for the second cumulants from which all the considered XAFS quantities have been provided. It has resulted based on the description of XAFS expressions derived using the anharmonic correlated Einstein model in terms of second cumulants. The many-body effects included in the present one-dimensional model are taken into account based on the first shell near neighbor contributions to the vibration between absorber and backscaterer atoms. Morse potential is assumed to describe the single-pair atomic interaction included in the anharmonic interatomic effective potential. Numerical and experimental results for Zn in hcp phase obtained by the present advanced method are found to be in good agreement with one another and with those measured at HASYLAB (DESY, Germany).

1. Introduction

X-ray Absorption Fine Structure (XAFS) has developed into a powerful technique for providing information on the local atomic structure and thermal effects of substances. The formalism for including anharmonic effects in XAFS is often based on cumulant expansion approach [1] from which the anharmonic XAFS function has resulted as

$$\chi(k) = F(k)\frac{e^{-2R/\lambda(k)}}{kR^2}\,\mathrm{Im}\left\{e^{i\Phi(k)}\exp\left[2ikR + \sum_n \frac{(2ik)^n}{n!}\sigma^{(n)}\right]\right\}, \qquad (1)$$

where F(k) is the real atomic backscattering amplitude, k and λ are the wave number and mean free path of photoelectron, respectively, Φ is the net phase shift, $R = \langle r \rangle$ with r

being the instantaneous bond length between absorber and backscatterer atoms, and $\sigma^{(n)}$ (n = 1, 2, 3, …) are the cumulants describing Debye-Waller factor (DWF).

Hence, the precise cumulants or DWFs are crucial to quantitative treatment of XAFS spectra where the even cumulants contribute to the amplitude, the odd ones to the phase of XAFS spectra, and for small anharmonicities, it is sufficient to keep the third and fourth cumulant terms [2]. Consequently, the lack of the precise cumulants has been one of the biggest limitations to accurate structural determinations (e.g., the coordination numbers and the atomic distances) [3] and to specify the other thermodynamic properties of substances [3-9] from XAFS experiments. Therefore, investigation of XAFS cumulants is of great interest.

The purpose of this work is to study not only the theoretical but also the experimental XAFS cumulants and thermal expansion coefficients of hcp (hexagonal close packed) crystals based the quantum statistically derived advanced method using that the calculations and measurements are necessary only for the second cumulants or mean square relative displacement (MSRD) from which all the considered XAFS quantities have been provided. The advances of this method have resulted (Section 2) based on the description of the analytical expressions for the considered XAFS quantities derived using the anharmonic correlated Einstein model (ACEM) in terms of second cumulants. The many-body effects included in the present one-dimensional model have been taken into account based on the first shell near neighbor contributions approach (FSNNCA). Morse potential is assumed to describe the single-pair atomic interaction included in the anharmonic interatomic effective potential. The present advanced method has also been applied to extracting and valuating the experimental XAFS parameters of Zn based on the experimental values of its second cumulants measured at the Beamline BL8, Synchrotron Light Research Institute (SLRI), Thailand. Numerical results for Zn in hcp phase (Section 3) are compared to the experimental values extracted by using the present advanced method and to those measured at HASYLAB (DESY, Germany) [10] which show good agreement. The conclusions on the obtained results are presented in Section 4.

2. XAFS Cumulants and Thermal Expansion Coefficient of Hcp Crystals

2.1. Theory

In order to include anharmonic effects, the Hamiltonian of system in the present theory includes the anharmonic interatomic effective potential expressed as

$$V_{eff}(x) \approx \frac{1}{2}k_{eff}x^2 + k_{3eff}x^3,\ x = r - r_0, \tag{2}$$

where k_{eff} is the effective local force constant and k_{3eff} is the cubic anharmonic parameter giving an asymmetry of the anharmonic effective potential, r and r_0 are the instantaneous and equilibrium distances between absorber and backscatterer atoms, respectively.

Using the FSNNCA which was successfully applied to bcc (body centered cubic) crystals [8], the anharmonic effective potential for hcp crystals has the form

$$V_{eff}(x) = V(x) + \sum_{i=1,2}\sum_{j\neq i} V\left(\frac{1}{2}x\hat{\mathbf{R}}_{12}\cdot\hat{\mathbf{R}}_{ij}\right), \tag{3}$$

where $\hat{\mathbf{R}}$ is unit vector; the sum i is over absorber (i = 1) and backscatterer (i = 2), and the sum j is over all their first shell near neighbors.

For hcp structure, each atom is bonded to 12 first shell near neighbors so that the anharmonic interatomic effective potential given by Eq. (3) contains not only the term V(x) describing the vibration between absorber and backscatterer atoms but also the other ones describing the projections of their pair-interactions with 22 first shell near neighbors along the bond direction except the absorber and backscatterer atoms themselves whose contributions are included already in V(x). Due to this projection as in Eq. (3) the many-body effects in the present one-dimensional model have been taken into account.

The Morse potential expanded up to the third order around its minimum

$$V(x) = D\left(e^{-2\alpha x} - 2e^{-\alpha x}\right) \approx D\left(-1 + \alpha^2x^2 - \alpha^3x^3\right) \tag{4}$$

is assumed to describe the single-pair atomic interaction included in the anharmonic effective potential, where α describes the width of the potential and D is the dissociation energy. Therefore, substituting this Morse potential into Eq. (3) and comparing the results to Eq. (2) the values of k_{eff}, k_{3eff} in terms of Morse parameters for hcp crystals included in all XAFS cumulants expressions are determined.

For deriving the XAFS cumulants we describe the anharmonic interatomic effective potential Eq. (3) for hcp crystals in terms of Morse potential parameters in the summation of the harmonic contribution and a perturbation δV due to the weak anharmonicity in XAFS as

$$V_{eff}(y) = \frac{1}{2}k_{eff}y^2 + \delta V(y),\ \delta V \cong 5D\alpha^2 ay + k_{3eff}y^3,\ y = x - a,\ \ a = \langle x\rangle. \tag{5}$$

The derivation of XAFS cumulants for hcp crystals in this work is using the ACEM based on quantum statistical theory [11] and the parameters of the anharmonic interatomic effective potentials given by Eqs. (3) and (5), as well as an averaging procedure using the canonical partition function Z and statistical density matrix ρ, e.g.,

$$\left\langle y^m \right\rangle = \frac{1}{Z} Tr\left(\rho\, y^m\right), \quad m = 1, 2, 3, \cdots \tag{6}$$

Atomic vibrations are quantized in terms of phonons, and anharmonicity is the result of phonon-phonon interaction, that is why we express y in terms of the annihilation and creation operators, $\hat{a}$ and $\hat{a}^+$, respectively

$$y \equiv a_0\left(\hat{a} + \hat{a}^+\right), \quad a_0 = \sqrt{\frac{\hbar\omega_E}{10D\alpha^2}}, \tag{7}$$

which have the following properties

$$\left[\hat{a}, \hat{a}^+\right] = 1,\ \hat{a}^+\left|n\right\rangle = \sqrt{n+1}\left|n+1\right\rangle,\ \hat{a}\left|n\right\rangle = \sqrt{n-1}\left|n-1\right\rangle,\ \hat{a}^+\hat{a}\left|n\right\rangle = n\left|n\right\rangle, \tag{8}$$

as well as use the harmonic oscillator state $\left|n\right\rangle$ as the eigenstate with the eigenvalue $E_n = n\hbar\omega_E$ for n being the phonon number, ignoring the zero-point energy for convenience.

Due to weak anharmonicity in XAFS, the canonical partition function in Eq. (6) can be expressed as

$$Z \cong Z_0 = \sum_n e^{-n\beta\hbar\omega_E} = \sum_{n=0}^{\infty} z^n = \frac{1}{1-z}, \quad z = \exp\left(-\theta_E / T\right). \tag{9}$$

Here, the correlated Einstein frequency ω_{E} and temperature θ_{E} for hcp crystals have the forms

$$\omega_E = \sqrt{\frac{10D\alpha^2}{M}}, \quad \theta_E = \frac{\hbar\omega_E}{k_B}, \tag{10}$$

where M is the atomic mass and k_{B} is Boltzmann constant.

Using the above results for the correlated atomic vibration and the procedure depicted by Eqs. (6) - (9), as well as the first-order thermodynamic perturbation theory [11], the temperature-dependent XAFS cumulants have been derived.

Based on the procedure depicted by Eq. (6) – (10) we derived the even moment expressing the second cumulant or MSRD

$$\sigma^2(T) = \left\langle y^2 \right\rangle = \sum_n e^{-n\beta\hbar\omega_E} \left\langle n\left|y^2\right|n\right\rangle,\ \beta = 1/k_B T, \tag{11}$$

and the odd moments expressing the first (m = 1) and third (m = 3) cumulants

$$\left\langle y^m \right\rangle = \frac{k_{eff}}{Z_0} \sum_{n,n'} \frac{e^{-\beta E_n} - e^{-\beta E_{n'}}}{E_n - E_{n'}} \left\langle n\left|\delta V(y)\right|n'\right\rangle \left\langle n'\left|y^m\right|n\right\rangle,\ m = 1, 3 \tag{12}$$

where the operations expressed by Eqs. (6) and (7) have been applied to calculate the matrix elements given in Eqs. (11) and (12).

Consequently, the XAFS expressions have resulted for the second cumulant or MSRD

$$\sigma^2(T) = \left\langle y^2 \right\rangle = \sigma_0^2 \frac{1+z(T)}{1-z(T)},\ \sigma_0^2 = \frac{\hbar\omega_E}{10D\alpha^2}, \tag{13}$$

for the first cumulant or net thermal expansion

$$\sigma^{(1)}(T) = a = \sigma_0^{(1)} \frac{1+z(T)}{1-z(T)} = \frac{\sigma_0^{(1)}}{\sigma_0^2}\sigma^2(T),\ \sigma_0^{(1)} = \frac{3\alpha}{4}\sigma_0^2, \tag{14}$$

and for the third cumulant or mean cubic relative displacement (MCRD)

$$\sigma^{(3)}(T) = \left\langle y^3 \right\rangle = \sigma_0^{(3)}\left[3\left(\frac{\sigma^2(T)}{\sigma_0^2}\right)^2 - 2\right],\ \sigma_0^{(3)} = \frac{\alpha}{2}\left(\sigma_0^2\right)^2 . \tag{15}$$

Moreover, the second cumulant given by Eq. (13) is harmonic while the experimental data always include the temperature-dependent anharmonic effects. That is why we introduce the total second cumulant or MSRD as

$$\sigma_{tot}^2(T) = \sigma^2(T) + \sigma_A^2(T), \tag{16}$$

which involves an anharmonic contribution

$$\sigma_A^2(T) = \beta_A(T)\left[\sigma^2(T) - \sigma_0^2\right], \tag{17}$$

containing the anharmonic factor

$$\beta_A(T) = \frac{9\alpha^2}{8}\sigma^2(T)\left[1 + \frac{3\alpha}{4R}\sigma^2(T)\left(1 + \frac{3\alpha}{4R}\sigma^2(T)\right)\right], \tag{18}$$

derived based on the relative volume change due to thermal expansion and also described in terms of second cumulant.

Futher, using the first cumulant given by Eq. (13), the expression for the thermal expansion coefficient has been derived and given by

$$\alpha_T(T) = \frac{1}{r}\frac{da}{dT} = \alpha_T^0 \frac{\left(\sigma^2(T)\right)^2 - \left(\sigma_0^2\right)^2}{T^2},\ \alpha_T^0 = \frac{15D\alpha^3}{4k_B r}. \tag{19}$$

In the above expressions $\sigma_0^{(1)}, \sigma_0^2, \sigma_0^{(3)}$ are zero-point energy contributions to three first XAFS cumulants $\sigma^{(1)}(T)$, $\sigma^2(T)$, $\sigma^{(3)}(T)$, respectively, and α_T^0 is the constant value which the thermal expansion coefficient approaches at high-temperatures.

Hence, the above derived expressions for the first, third

cumulants and thermal expansion coefficient $\sigma^{(1)}$, $\sigma^{(3)}$ and α_T, respectively, as well as the total second cumulant given by Eqs. (16) – (18) including anharmonic effects have been presented in terms of second cumulant σ^2 or MSRD. Such description is useful to create the present quantum statistical advanced method based on that the calculations and measurements are necessary only for the second cumulants from which the first, third cumulants, thermal expansion coefficient and other XAFS parameters can be provided. This is the advantage of the present advanced method leading to the effective reduction and simplification of XAFS calculations and measurements shown in the next sections.

2.2. Experimental

The measurements of the values of second cumulants or MSRDs of Zn in hcp phase at 300 K, 400 K, 500 K and 600 K have been performed at the Beamline BL8, SLRI (Thailand). It is the routinely operated for X-ray absorption spectroscopy (XAS) in an immediate photon energy range (1.25 – 10 keV). The experimental set-up conveniently facilitates XAS measurements in transmission and fluorescence-yield modes at several K-edges of elements ranging from Magnesium to Zinc [12]. The experimental values of the first, third cumulants and thermal expansion coefficients of Zn at 300 K, 400 K, 500 K, 600 K have been extracted from the measured values of the second cumulants using the present method based on the description of these quantities in terms of second cumulant presented in Section 2.1. The obtained experimental results will be presented in Section 3 compared to the calculated results and to those measured in HASYLAB (DESY, Germany) at 77 K and 300 K [10].

3. Numerical Results Compared to Experiment and Discussions

Now the expressions derived in the Section 2.1 are applied to numerical calculations for Zn in hcp phase using its Morse potential parameters [13] D = 0.1700 eV, α = 1.7054 $Å^{-1}$ which were obtained using experimental values for the energy of sublimation, the compressibility, and the lattice constant.

Figure 1 illustrates good agreement of first cumulant $\sigma^{(1)}(T)$ of Zn calculated using the present theory with the experimental values at 300 K, 400 K, 500 K and 600 K extracted using the present advanced method and with those measured in HASYLAB (DESY, Germany) at 77 K and 300 K [10]. Note that from this first cumulant we can also obtain temperature dependence of the first shell near neighbor distance based on the expression $R(T) = R(0) + \sigma^{(1)}(T)$.

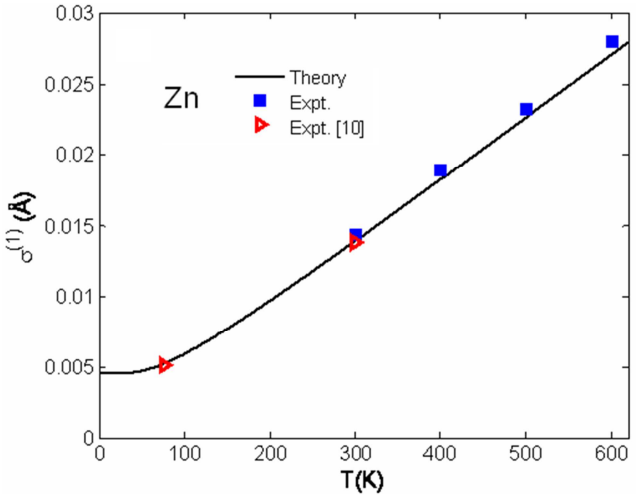

Figure 1. *Temperature dependence of first cumulant $\sigma^{(1)}(T)$ of Zn calculated using the present theory compared to the experimental values at 300 K, 400 K, 500 K and 600 K extracted using the present advanced method and with those measured in HASYLAB (DESY, Germany) at 77 K and 300 K [10].*

The good agreement of total and harmonic second cumulants $\sigma^2_{tot}(T)$, $\sigma^2(T)$, respectively, of Zn calculated using the present theory with the experimental values at 300 K, 400 K, 500 K, 600 K obtained in this work and with those measured in HASYLAB (DESY, Germany) at 77 K and 300 K [10] is presented in Figure 2. Here, $\sigma^2_{tot}(T)$ is a little different from $\sigma^2(T)$ at temperatures greater than the room temperature due to the anharmonic contributions.

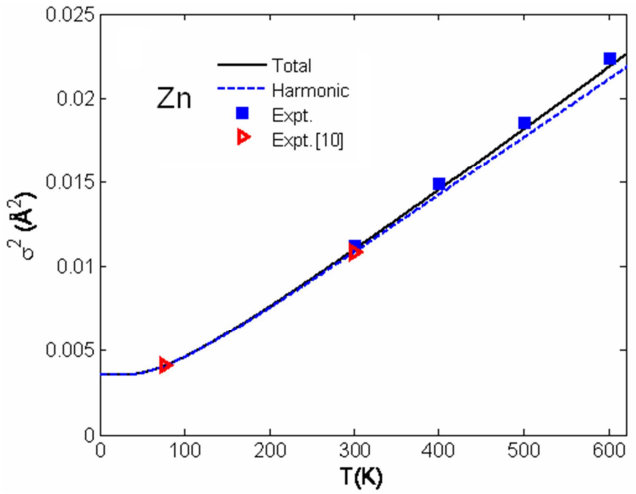

Figure 2. *Temperature dependence of total and harmonic second cumulants $\sigma^2_{tot}(T)$ and $\sigma^2(T)$, respectively, of Zn calculated using the present theory compared to the experimental values at 300 K, 400 K, 500 K and 600 K obtained in this work and with those measured in HASYLAB (DESY, Germany) at 77 K and 300 K [10].*

Figure 3 shows good agreement of temperature dependence of third cumulant $\sigma^{(3)}(T)$ of Zn calculated using the present theory with the experimental values at 300 K, 400 K, 500 K and 600 K extracted using the present advanced method and with those measured in HASYLAB (DESY, Germany) at 77 K and 300 K [10].

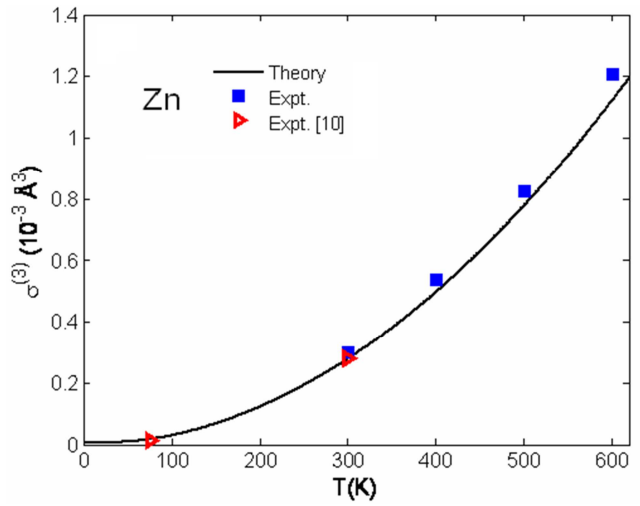

Figure 3. *Temperature dependence of third cumulant $\sigma^{(3)}(T)$ of Zn calculated using the present theory compared to the experimental values at 300 K, 400 K, 500 K and 600 K extracted using the present advanced method and to those measured in HASYLAB (DESY, Germany) at 77 K and 300 K [10].*

Moreover, temperature dependence of (Figure 4) anharmonic contributions $\sigma_A^2(T)$ to second cumulant or MSRD and (Figure 5) anharmonic factor $\beta_A(T)$ of Zn calculated using the present theory agrees well with the experimental values at 300 K, 400 K, 500 K, 600 K and with those measured in HASYLAB (DESY, Germany) at 77 K and 300 K [10]. Here $\beta_A(T)$ characterizes percentage of the anharmonic contributions at each temperature. These values are normally difficult to be directly measured, but using the present advanced method they have been calculated and extracted from the calculated and measured second cumulants.

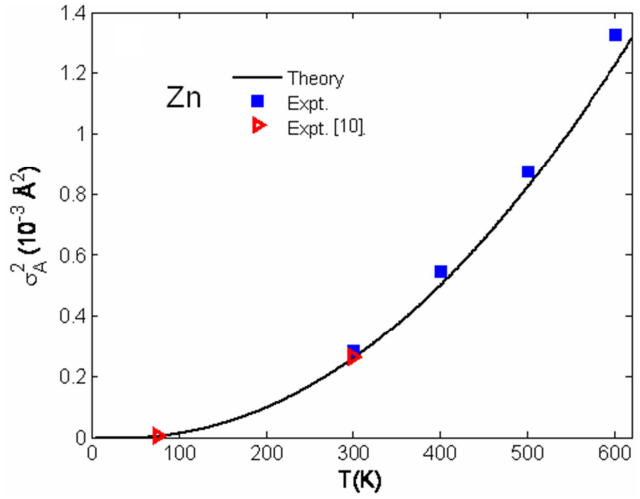

Figure 4. *Temperature dependence of anharmonic contributions $\sigma_A^2(T)$ to second cumulant of Zn calculated using the present theory compared to the experimental values at 300 K, 400 K, 500 K, 600 K extracted using the present advanced method and to those measured in HASYLAB (DESY, Germany) at 77 K and 300 K [10].*

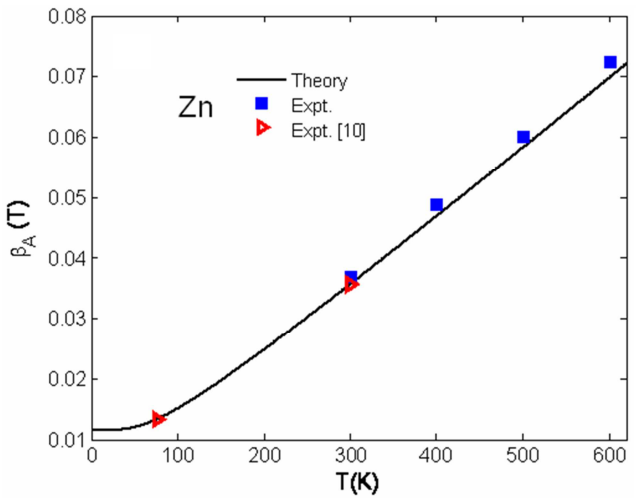

Figure 5. *Temperature dependence of anharmonic factor $\beta_A(T)$ of Zn calculated using the present theory compared to the experimental values at 300 K, 400 K, 500 K, 600 K extracted using the present advanced method and to those measured in HASYLAB (DESY, Germany) at 77 K and 300 K [10].*

Temperature dependence of thermal expansion coefficient $\alpha_T(T)$ of Zn calculated using the present theory (Figure 6) agrees well with the experimental values at 300 K, 400 K, 500 K and 600 K extracted using the present advanced method and with those measured in HASYLAB (DESY, Germany) at 77 K and 300 K [10]. Here, the theoretical and experimental thermal expansion coefficients of Zn approach the constant values at high-temperatures as it was obtained for the other crystal structures [9].

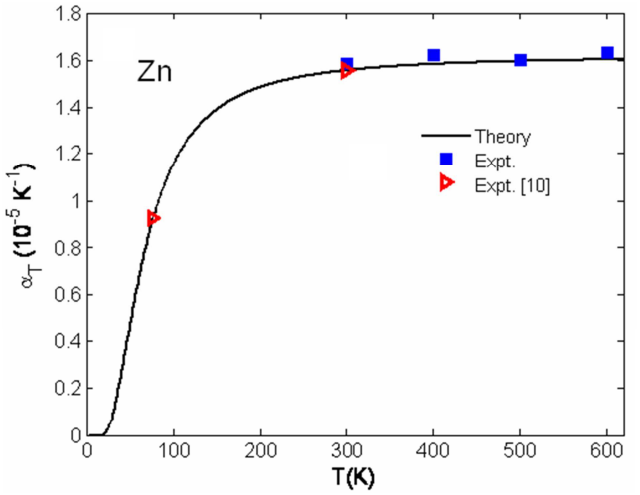

Figure 6. *Temperature dependence of thermal expansion coefficient $\alpha_T(T)$ of Zn calculated using the present theory compared to the experimental values at 300 K, 400 K, 500 K and 600 K extracted using the present adanced method and to those measured in HASYLAB (DESY, Germany) at 77 K and 300 K [10].*

Note that in the above obtained results the first cumulant (Figure 1) and second cumulant (Figure 2) are linearly proportional to the temperature T and the third cumulant (Figure 3) to T^2 at high-temperatures, and all they contain zero-point energy contributions at low-temperatures, a quantum effect, as for the other crystal structures [9].

The cumulant ratios $\alpha_T r T\sigma^2/\sigma^{(3)}$ and $\sigma^{(1)}\sigma^2/\sigma^{(3)}$ are often considered as the standards for cumulant studies [9, 10, 14] and to identify the temperature above which the classical limit is applicable [9]. Figures 7 and 8 illustrate good agreement of temperature dependence of $\alpha_T r T\sigma^2/\sigma^{(3)}$ and $\sigma^{(1)}\sigma^2/\sigma^{(3)}$, respectively, of Zn calculated using the present theory with the experimental values at 300 K, 400 K, 500 K and 600 K extracted using the present advanced method and with those measured in HASYLAB (DESY, Germany) at 77 K and 300 K [10]. The theoretical and experimental results of these ratios show that above the Einstein temperature (θ_E = 206 K calculated using the present theory for Zn) they reach the classical value [7, 14] of 1/2 so that the classical limit is applicable.

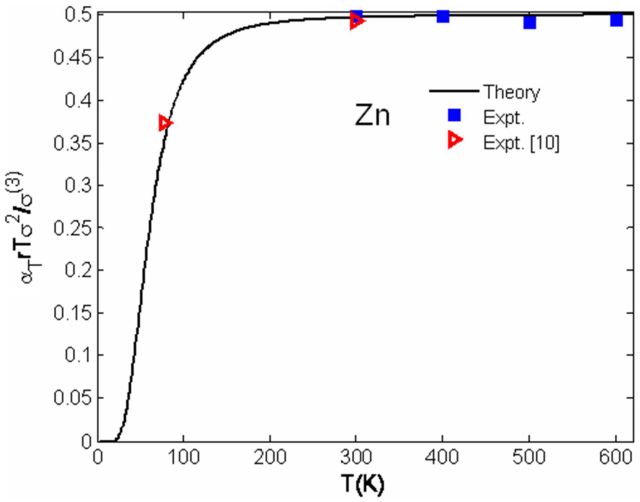

Figure 7. *Temperature dependence of cumulant ratio $\alpha_T r T\sigma^2/\sigma^{(3)}$ of Zn calculated using the present theory compared to the experimental values at 300 K, 400 K, 500 K and 600 K extracted using the present advanced method and to those measured in HASYLAB (DESY, Germany) at 77 K and 300 K [10].*

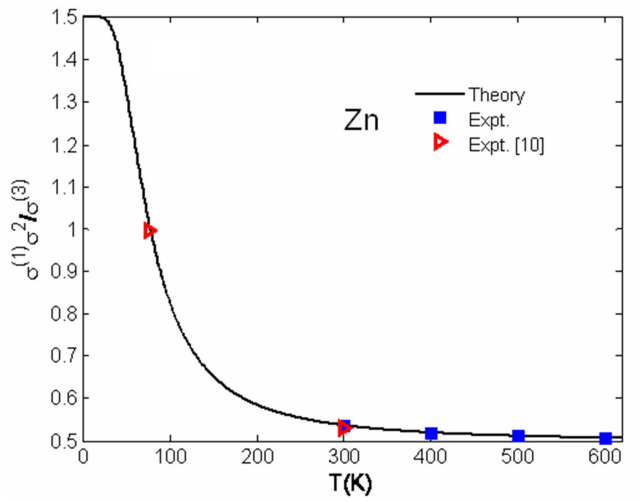

Figure 8. *Temperature dependence of cumulant ratio $\sigma^{(1)}\sigma^2/\sigma^{(3)}$ of Zn calculated using the present theory compared to the experimental values at 300 K, 400 K, 500 K and 600 K extracted using the present advanced method and to those measured in HASYLAB (DESY, Germany) at 77 K and 300 K [10].*

The XAFS cumulants parametrize the asymmetric distribution of interatomic distances, and can be connected to the force constants of a one-dimensional effective pair potential [2-10]. In particular, the first three cumulants measure the average value, the variance, and the asymmetry of the distribution, respectively [16]. Both the first and third cumulants have often been considered equally sensitive to thermal expansion [17]. This equivalence, which is valid for a one-dimensional system, where the average distance is solely modified by the asymmetry of the interaction potential, was not confirmed by accurate XAFS measurements of nearest neighbors distances in several simple crystals [18-20]. Actually, the first XAFS cumulant is lager than the distance between the centers of the probability distribution functions, owing to the effect of atomic vibrations perpendicular to the bond direction [21, 22] and its temperature dependence is stronger than the thermal expansion measured by Bragg diffraction or by macroscopic techniques. The difference between XAFS and crystallographic thermal expansion can be attributed to the MSRD component perpendicular to the bond direction [3, 18]. Unfortunately, based on the good agreement XAFS cumulants of Zn calculated using the present theory with the experimental values extracted by using the present advanced method and with those measured in HASYLAB (DESY, Germany) the contribution of the perpendicular MSRD to the second cumulant of Zn can be considered negligible.

Consequently, the second cumulant describing MSRD is primary a harmonic effect plus small anharmonic contributions which appear only at high-temperatures. But the first cumulant describing the net thermal expansion or lattice disorder, the third cumulant or MCRD describing the asymmetry of pair atomic distribution function and the thermal expansion coefficient are entirely anharmonic effects because they appear due to including the cubic anharmonic effective potential parameter. We also used the present advanced method and the measured second cumulants of Zn at 300 K, 400 K, 500 K and 600 K to reproduce all the considered experimental values. The obtained results agree well with the measured data at these temperatures presented in the above figures. Hence, the obtained theoretical and experimental XAFS quantities contribute to the valuation and analysis of thermodynamic properties and anharmonic effects of Zn in hcp phase. Moreover, based on Eq. (1) the above obtained precise cumulants contribute to the accurate structural determination of the crystal using its XAFS spectra including anharmonic effects and their Fourier transform magnitudes [15].

4. Conclusions

In this work, the advances in the theoretical and experimental XAFS studies of DWFs presented in terms of cumulant expansion up to the third order and thermal expansion coefficient of hcp crystals have been performed. The obtained results contribute to the valuation and analysis of the thermodynamic properties and anharmonic effects, as

well as to the accurate structural determination of the considered crystal.

The most advantageous development in this work is the present quantum statistically derived advanced method using which all the considered theoretical and experimental XAFS quantities have been obtained and extracted from the calculated and measured second cumulants or MSRDs. It has significantly simplified and reduced the XAFS calculations and measurements.

The obtained temperature-dependent theoretical and experimental XAFS quantities have been in detail analyzed and valuated. They include the evident anharmonic effects and satisfy all their fundamental properties, as well as reach the classical values at high-temperatures and contain zero-point energy contributions at low-temperatures, a quantum effect.

The good agreement between the theoretical results calculated using the present theory and the experimental data extracted using the present advanced method, as well as their good agreement with those measured in the other research for Zn illustrate the simplicity and efficiency of the present derived method in XAFS data analysis and in materials studies.

References

[1] E. D. Crozier, J. J. Rehr, and R. Ingalls, in *X-ray Absorption*, edited by D. C. Koningsberger and R. Prins (Wiley, New York, 1988). Chap. 9.

[2] J. M. Tranquada and R. Ingalls, Extended x-ray-absorption fine-structure study of anharmonicity of CuBr, Phys. Rev. B 28, 3520 (1983).

[3] F. D. Vila, J. J. Rehr, H. H. Rossner., H. J. Krappe, Theoretical x-ray absorption Debye-Waller factors, Phys. Rev. B 76, 014301 (2007).

[4] N. V. Hung, V. V. Hung, H. K. Hieu, R. R. Frahm, Pressure effects in Debye-Waller factors and in EXAFS, Phys. B 406, 456 (2011).

[5] N. V. Hung, C. S. Thang, N. C. Toan, H. K. Hieu, Temperature dependence of Debye-Waller factors of semiconductors. VAC. 101, 63 (2014).

[6] N. V. Hung, Pressure-Dependent Anharmonic Correlated Einstein Model XAFS Debye-Waller Factors. J. Phys. Soc. Jpn. 83, 024802 (2014).

[7] N. V. Hung, T. S. Tien, N. B. Duc, D. Q. Vuong, High-order expanded XAFS Debye-Waller factors of hcp crystals based on classical anharmonic correlated Einstein model. Mod. Phys. Lett. B 28, 1450174 (2014).

[8] N. V. Hung, T. T. Hue, H. D. Khoa, D. Q. Vuong, Anharmonic correlated Debye model high-order expanded interatomic effective potential and Debye-Waller factor of bcc crystals, Phys. B 503, 174 (2016).

[9] N. V. Hung and J. J. Rehr, Anharmonic correlated Einstein model Debye-Waller factors. Phys. Rev. B 56, 43 (1997).

[10] N. V. Hung, T. S. Tien, L. H. Hung and R. R. Frahm, Anharmonic Effective Potential, Local Force Constant and EXAFS of HCP Crystals: Theory and Comparison to Experiment. Int. J. Mod. Phys. B 22, 5155 (2008).

[11] R. P. Feynman, *Statistical Mechanics*, edited by Jacob Shaham, W. A. Benjamin, INC. Advanced book Program, Reading, Massachusetts, 1972.

[12] W. Klysubun, P. Sombunchoo, W. Deenam, C. Komark, Performance and status of beamline BL18 at SLRI for X-ray absorption spectroscopy, J. Synchrotron Rad. 19, 930 (2012).

[13] N. V. Hung, A method for calculation of Morse potential for fcc, bcc, hcp crystals applied to Debye-Waller factors and equation of state, Commu. in Phys. (CIP) 14 (1), 7 (2014).

[14] A. Stern, P. Livins, and Zhe Zhang, Thermal vibration and melting from a local perspective, Phys. Rev. B 43, 8850 (1991).

[15] N. V. Hung, N. B. Duc, R. R. Frahm, A new anharmonic factor and EXAFS including anharmonic contributions, J. Phys. Soc. Jpn. 72, 1254 (2003).

[16] P. Fornasini, S. a Beccara, G. Dalba, R. Grisenti, A. Sanson, M. Vaccari and F. Rocca, EXAFS measurements of Cu: Local dynamics, anharmonicity, and thermal expansion, Phys. Rev. B 70, 174301 (2004).

[17] L. Tröger, T. Yokoyama, T. Arvanitis, T. Lederer, M. Tischer, K. Baberschke, Phys. Rev. B 49, 888 (1994).

[18] G. Dalba, P. Fornasini, R. Grisenti, J. Purans, Phys. Rev. Lett. 82, 4240 (1999).

[19] P. Eisenberger and G. S. Brown, Solid State Commun. 29, 481 (1979).

[20] G. Dalba, P. Fornasini, R. Gotter, F. Rocca, Phys. Rev. B 52, 149 (1995).

[21] B. T. M. Wilis and A. W. Pryor, *Thermal Vibrations in Crystallography* (Cambtige University Press, Cambrige, 1975).

[22] T. Ishii, J. Phys.: Condens. Matter 4, 8029 (1992).